Entropy analysis of water/water thermoelectric heat pumps: design considerations

Ibrahim Neya, Julien Ramousse, Maxime Perier-Muzet

Entropy analysis of water/water thermoelectric heat pumps: design considerations

I. Neya[a], J. Ramousse[a], M. Perier-Muzet[a]

[a] LOCIE, Université de Savoie, Le Bourget du Lac 73376, France. julien.ramousse@univ-savoie.fr

Abstract:

This work aims to propose routes for thermoelectric heat pump design based on thermodynamic approach. The system considered is composed of a thermoelectric module sandwiched between two water multi-channels heat exchangers. The optimized variables considered in this study are: the thermoelectric leg number, their length and section, and the number of channels in both heat exchangers and their length and diameter. Entropy generation due to dissipative phenomena are evaluated and discussed. The following contributions are identified: thermal conduction and Joule effect in the thermoelectric module, and heat transfer and viscous dissipation in both heat exchangers. This study highlights optimal design ratios in the thermoelectric module. To reduce the thermoelectric material volume it is recommended to reduce the thermoelectric leg length. As the optimal heat exchanger design results in low Reynolds number heat exchanger with high footprint, the authors propose to design heat exchangers for transitional regime, corresponding to a local minimum of the entropy generation rate. Although the entropy generation in the heat exchangers is low compared to that in the thermoelectric module (mainly by Joule effect), the heat exchanger design highly impacts the global system performance.

Keywords:

Second law analysis ; Entropy Generation Minimization (EGM) ; Energy conversion ; heat exchanger

1. Introduction

Since thermoelectric phenomena were discovered at the end of 19th century, many thermoelectric applications have been considered to convert electric power to thermal power, and inversely. These thermoelectric devices are generally used when the target applications impose minimum space, noise, weight or an environment with substantial mechanical constraints. Today, this technology tends to compete with the classical vapour compression heat pumps. As no compressors or refrigerant are used in thermoelectric heat pumps (THPs), they are more reliable (no maintenance is necessary) and eco-friendly [5]. The coefficient of performance (COP) of THPs depends on the thermoelectric efficiency of the module, but also on the thermal coupling between the thermoelectric module and the heat source/sink. Their performance is still lower than vapour compression devices, except when the temperature difference is only a few degrees [4]. Thus, more recently THPs have been used for heating and cooling devices for buildings [6-9], since thermal power needs and the temperature difference are decreasing with the advent of low-temperature heating devices. Particular attention is paid to this type of application, for which the constraint related to the compactness of the THP is no longer pertinent. In these applications, low thermal power density can be achieved leading to reconsider the classical THP design originally aimed for high power density.

This study analyses the optimal design for water/water THPs in steady-state conditions in an attempt to increase the system's performance. The THP considered is composed of a thermoelectric module sandwiched between two water heat exchangers, for water/water building heat pump applications. The thermoelectric module considered is classically composed of several legs, made of bulk semiconductor materials (mainly Bismuth Telluride for working temperatures close to the ambient) and connected in series electrically and in parallel thermally. Parallel multi-channels heat exchangers are used to transfer heat flux from the thermoelectric module to the heat source and heat sink.

Many studies have been lead on the thermoelectric module itself to characterize their intrinsic performances. Thermodynamic analysis in the thermoelectric material is presented in [10]. Using

numerical and analytical models, many authors [11] [12] [18] showed that several designs can provide similar performance. In particular, the number of legs, their section and their length are closely related so as to meet a given thermal power demand with maximum COP, depending on the heat exchangers thermal resistances. These optimal ratios are also derived in this paper and discussed taking into account additional manufacturing criteria. On the other hand, a detailed thermodynamic analysis of heat exchangers is proposed in [13]. Many studies have been lead on the heat exchangers technologies to be associated to the thermoelectric module. However, few studies are carried out on the design of the whole system coupled to its sources, including the thermoelectric module and the two heat exchangers. In the case of a thermoelectric generator, the whole system optimization proposed in [20] shows that the thermoelectric module and its associated heat exchanger designs are closely related. The authors thus propose to co-optimize the thermoelectric module and the heat exchangers designs, based on entropy analysis.

This paper proposes a thermodynamic analysis of the THPs dissipation to help at their design. The study includes the thermoelectric module and the hot and cold heat exchangers used to transfer heat from the thermoelectric module to the hot source and to the cold sink. Each dissipative phenomenon in the system is identified and evaluated. Their comparison and analysis help to propose realistic THP design depending on the thermal power demand, the fluid operating temperatures and the material properties.

2. Model

The system considered is composed of the thermoelectric module sandwiched between two multi-channels heat exchangers as presented in figure 1.

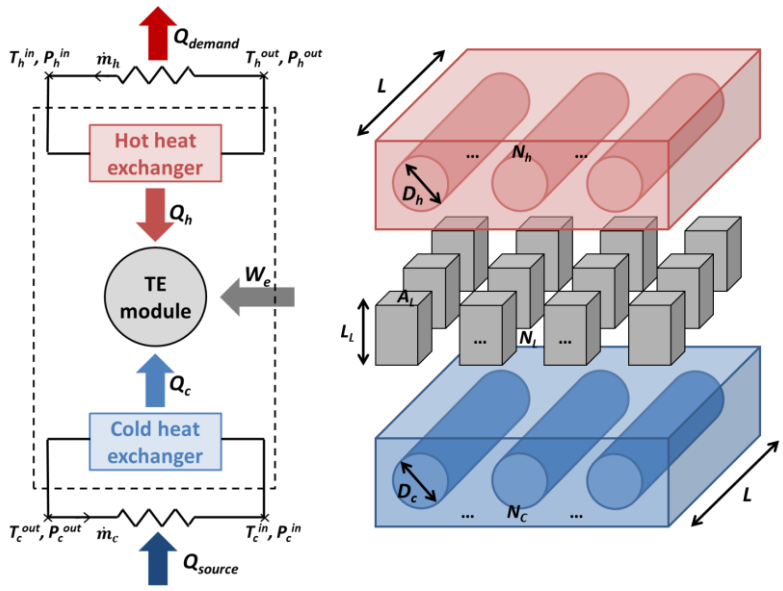

Fig. 1. Schematic representation of the system.

The engineering optimization problem can be formulated as follow: What is the best system design to reach a thermal demand with maximum performances? This formulation assumes that the thermoelectric material and fluid properties are known. The operating conditions, such as the inlet/outlet temperatures in both heat exchangers and the thermal demand, have to be defined. The design variables considered in this study are:

- In the thermoelectric module: the leg length L_L, its section A_L and their number N_L.
- In both heat exchangers: The number of channel N_h and N_c and their diameter D_h and D_c, for the hot and cold heat exchangers, respectively. The channel length L is assumed equal in both heat exchangers.

The model was simplified according to the following assumptions that help to interpret the main evolution of the system regarding to the internal dissipative phenomena.

- Uniform temperature is assumed in both heat exchangers, taken equal to the outlet temperature. This assumption tends to under-estimate heat flux transferred in the heat exchanger.
- By the way, the hot and cold temperatures are assumed uniform at the thermoelectric junctions. This assumption helps to set homogeneous operating conditions to the thermoelectric module. For further precision, a space meshing would be needed.
- Total heat flux is conserved at the thermoelectric module and heat exchangers interface, independently of their respective area (total thermoelectric legs surface vs footprint of the heat exchangers), meaning thermal constriction resistances are neglected.
- Pressure drops through the heat exchangers distributor and collector are not taken into account in this study. This additional dissipative phenomenon leads to reduce the channels number in the heat exchangers, as the entropy generation associated to viscous dissipation would increase, leading to shift the optimal operating conditions.

2.1. Thermoelectric module

The thermoelectric description is based on the model originally proposed by Ioffe [14]. Let's consider a thermoelectric module composed of N_L thermoelectric legs connected in series electrically and in parallel thermally. The legs, of section A_L and length L_L, are made of bulk semiconductor materials (mainly Bismuth Telluride for working temperatures close to the ambient temperature). The leg properties (Seebeck coefficient α, thermal conductivity λ and electrical resistivity ρ) are evaluated at a mean temperature $T_m = \frac{T_h^{TE}+T_c^{TE}}{2}$, where T_h^{TE} and T_c^{TE} are the hot and cold junction temperatures, respectively. This assumption remains valid as long as the Joule effect is not excessive [15]. Besides, the temperature difference between T_h^{TE} and T_c^{TE} is usually low when thermoelectric elements operate in THP mode, so T_m is close to the mean side temperatures. The present study is based on the expressions for Bi_2Te_3 bulk properties depending on the temperature (Table 1), given by Riffat et al. [16].

Table 1: Bi2Te3 properties vs. the mean temperature [16]

Thermal conductivity	$\lambda(T) = \left(62,605 - 277.7 \cdot T + 0.4131 \cdot T^2\right) \cdot 10^{-4}$	[W/(m K)]
Electrical resistivity	$\rho(T) = \left(5,112 + 163.4 \cdot T + 0.6279 \cdot T^2\right) \cdot 10^{-10}$	[Ω.m]
Seebeck coefficient	$\alpha(T) = \left(22,224 + 930.6 \cdot T - 0.9905 \cdot T^2\right) \cdot 10^{-9}$	[V/K]

Assuming that Joule effect is fairly distributed between hot and cold junctions in steady state, the released and absorbed heat fluxes at the thermoelectric junctions, respectively Q_h and Q_c, are the sum of three contributions: Seebeck effect, Joule effect and thermal conduction.

$$Q_c = -Q_c^{Seebeck} + Q^{Joule} + Q^{Cond} = N_L\left(-\alpha_m \cdot I \cdot T_c^{TE} + \frac{1}{2}R \cdot I^2 + K \cdot \Delta T\right) \quad (1)$$

$$Q_h = Q_h^{Seebeck} + Q^{Joule} - Q^{Cond} = N_L\left(\alpha_m \cdot I \cdot T_h^{TE} + \frac{1}{2}R \cdot I^2 - K \cdot \Delta T\right) \quad (2)$$

The electrical resistance $R = {}^{L_L}/_{A_L}\,\rho$ and the thermal conductance $K = {}^{A_L}/_{L_L}\,\lambda$ of the legs are determined by integration on a leg of length L_L and section A_L. In accordance with the first law of

thermodynamics, the electrical power W_e to supply to the thermoelectric module is deduced from Q_h and Q_c:

$$W_e = -Q_h - Q_c = -N_L\left(R \cdot I^2 + \alpha_m \cdot I \cdot \Delta T\right) \tag{3}$$

The heating COP is defined as the ratio between the released heat and the electrical power supplied to the TE:

$$COP = \frac{Q_h}{|W_e|} = \frac{\alpha_m \cdot I \cdot T_h + \frac{1}{2} R \cdot I^2 - K \cdot \Delta T}{R \cdot I^2 + \alpha_m \cdot I \cdot \Delta T} \tag{4}$$

Applying the second law of thermodynamics to the thermoelectric module leads to:

$$\frac{Q_h}{T_h} + \frac{Q_c}{T_c} + S_{gen}^{TE} = 0 \tag{5}$$

With respect to (3) and (5), the COP is closely related to the entropy generation in the system by:

$$COP = \frac{{Q_h}/{T_c}}{{Q_h}/{T_c} - {Q_h}/{T_h} - S_{gen}^{TE}} \tag{6}$$

As demonstrated by [10], the entropy generation in thermoelectric systems is the sum of two contributions: (i) Thermal conduction and (ii) Joule effect, so that:

$$S_{gen}^{TE} = S_{gen}^{Cond} + S_{gen}^{Joule} > 0 \tag{7}$$

Both contributions to the entropy generation are given by their respective entropy flux at temperatures T_h^{TE} and T_c^{TE}:

$$S_{gen}^{Cond} = Q^{Cond}\left(\frac{1}{T_c^{TE}} - \frac{1}{T_h^{TE}}\right) > 0 \tag{8}$$

$$S_{gen}^{Joule} = Q^{Joule}\left(\frac{1}{T_c^{TE}} + \frac{1}{T_h^{TE}}\right) > 0 \tag{9}$$

Note that these expressions are coherent with the first and second law expressions.

2.2. Heat exchangers

Two heat exchangers are needed to transfer heat from the source/sink to the thermoelectric module at the hot and cold sides, respectively. Heat transfer is ensured by water flow in several parallel multi-channels in both heat exchangers, as presented in Figure 1.

The first law of thermodynamics applied to an incompressible fluid leads to:

$$Q + \dot{m}\left[Cp\left(T^{in} - T^{out}\right) + \frac{\left(P^{in} - P^{out}\right)}{\rho}\right] = 0 \tag{10}$$

This equation is used for both hot and cold heat exchangers with subscripted notations *c/h*. The pressure drop across each heat exchanger is evaluated thanks to following classical correlations [17] for fully developed flow in channel:

For laminar regime: $f = \frac{64}{Re}$ if $Re < 2300$

For turbulent regime: $f = \frac{1}{(0.790 ln(Re) - 1.64)^2}$ if $3000 < Re < 5.10^6$

Concerning the transitional regime, for value of *Re* included in the range [2300; 3000], *f* is linearized for numerical convergence purpose. Note that the Reynolds number $Re = \frac{\rho v D}{\mu}$ is estimated with the mini-channel diameter *D* and the flow velocity $v = \frac{\rho \dot{m}^{ch}}{\pi D^2/4}$, assuming an equidistribution of the total mass flow between the channels, so that $\dot{m}^{tot} = N^{ch}\dot{m}^{ch}$. The pressure drops is then evaluated with respect to the friction factor *f*, as:

$$\Delta P = P^{in} - P^{out} = f\frac{L}{D}\rho\frac{v^2}{2} \quad (11)$$

Thermal transfer through the heat exchangers results in a thermal resistance between the junction temperature and the fluid temperature, mainly caused by convection. Thermal conduction in the heat exchanger bulk is neglected as its contribution to the global thermal resistance is very low compared to convective contribution (for high conductive material, such as copper or stainless steel). Furthermore, the temperature is assumed homogeneous through the heat exchangers and equals the outlet temperature T_{out}, for simulation purpose. Considering only convective heat transfer in the mini-channels, it can be written:

$$Q = hA_{ex}(T_b - T_{out}) = \frac{(T_b - T_{out})}{R_{th}} \quad (12)$$

Where T_b is the temperature of each heat exchanger basis, taken equal to the hot and cold junction temperatures for the hot and cold heat exchangers, respectively. The exchange area is $A_{ex} = \pi DNL$ and the footprint area of the heat exchanger is $A_{hx} = 2DNL$, assuming the *N* channels of diameter *D* and length *L* are spaced regularly with an interstice equal to their diameter *D*.

The convective heat coefficient is evaluated thanks to the common correlation of literature [17]:

For laminar regime: $Nu = 4{,}36$ if $Re < 2300$

For turbulent regime: $Nu = 0{,}023Re^{0,8}Pr^{0,4}$ if $Re > 1.10^4$

With $Nu = {}^{hD}/_{\lambda}$ and $Pr = 7$ for water around ambient temperature. As for the friction factor *f*, a linear interpolation is used for transitional regime.

Applying the second law of thermodynamics to the heat exchanger system leads to:

$$\frac{Q}{T_b} + \dot{m}\Delta S + S_{gen}^{HX} = 0 \quad (13)$$

Where the entropy variation of water from the inlet to the outlet is: $\Delta S = Cp.\ln\left({}^{T_{in}}/_{T_{out}}\right)$.

As detailed in [13], the entropy generation in the heat exchanger is caused by two additional dissipative phenomena: heat transfer and viscous friction. Their respective contributions to the global entropy generation in both heat exchangers are:

$$S_{gen}^{th} = Q\left(\frac{1}{T_{out}} - \frac{1}{T_b}\right) > 0 \quad (14)$$

$$S_{gen}^{\Delta P} = \dot{m}Cp.ln\left(\frac{\Delta P}{\rho CpT_{in}} + 1\right) > 0 \quad (15)$$

Note that these expressions are coherent with the first and second law expressions, for low temperature difference and pressure drop along the heat exchanger.

3. Results and discussion

3.1. Simulation conditions

Based on the mathematical model presented in the previous section, simulation tools have been developed with the software Engineer Equation Solver EES for both heat exchangers and thermoelectric module.

Simulations were performed considering operating conditions closed to a water/water thermoelectric heat pump coupled to a ground source heat exchanger (as the cold source) and used for low temperature building heating (fig. 1).The whole system has to supply a given thermal power (Q_{demand}) to meet the building demand. For these simulations, the heat exchangers fluid inlet temperature (T^{in}) and pressure (P^{in}) have been set (for both hot and cold sides). The temperature difference from the inlet to the outlet in the heat exchangers is usually few K for this kind of application and has been set at 5 K. Consequently, the temperatures $\left(T_h^{TE} \text{ and } T_c^{TE}\right)$ and the thermal flux $\left(Q_h \text{ and } Q_c\right)$ at the

thermoelectric legs and heat exchangers interfaces are not imposed and are determined by the thermal coupling between these components. The operative conditions considered in this study are summarized in table 2. The water thermo physical properties have been considered constant.

Table 2: Main THP operative parameters

Thermal demand	Q_{demand}	3000 W
Fluid temperature at the hot exchanger inlet	T^{in}_{h}	298.15 K
Fluid temperature at the cold exchanger inlet	T^{in}_{c}	283.15 K
Fluid inlet pressure in the exchangers	P^{in}_{hx}	202650 Pa
Temperature difference between exchangers inlet and outlet	$\Delta T_{hx} = \left\| T^{in}_{hx} - T^{out}_{hx} \right\|$	5 K

In order to determine the optimal design of the entire system, numerical sensibility analyses have been performed on the heat exchanger and the thermoelectric module. Moreover, an optimization procedure has been carried out to determine the optimal geometry of the thermoelectric module for different heat exchanger designs. The objective function to minimize is the entropy generation in the system. The optimization procedure used for this study is the Golden Section Search algorithm available in the EES solver software.

3.2. Heat exchanger analysis

Two competitive dissipative phenomena, associated to heat transfer and to viscous friction, occur in a heat exchanger. The optimal design of a heat exchanger is thus a compromise between heat transfer intensification and viscous friction reduction.

To perform the heat exchanger analysis the thermal power (Q) has been set to 3000 W and the inlet and outlet fluid temperature (T^{in}_{hx} and T^{out}_{hx}) are equal respectively to 298.15 K and 303.15 K.

The Figure 2(a) plots the total heat exchanger entropy generation S_{gen}^{hx} vs the heat exchanger footprint area A_{hx} for different pipe diameter. The corresponding entropy generation ratio in the heat exchanger $\left(R^{hx}_{Sgen} = S^{th}_{gen} / S^{\Delta P}_{gen} \right)$ is plotted in figure 2(b). The pipe length is kept constant to 5 m. Based on the model presented above, it can be shown that the heat exchanger footprint area A_{hx} is inversely proportional to the Reynolds number in the pipe Re, for a given pipe length.

Even if a pipe diameter increase reduces the entropy generation by friction, the corresponding increase of the entropy generation by heat transfer results in a global entropy increase in the heat exchanger, as confirmed by Figure 2(a) and (b). The figure 2(a) shows that there is an optimal diameter which is a compromise between this to dissipative phenomena. The optimal pipes diameter with these operative conditions is between 1.10^{-3} m and 5.10^{-3} m.

As expected, whatever the pipe diameter the minimum entropy generation is reached for the higher heat exchanger area (fig. 2(a)). In these cases of low Reynolds numbers, the entropy generation by friction is very low compared to that generated by heat transfer (fig. 2(b)). For each pipe diameter, a local maximum of entropy generation is reached at the laminar/transitional regime transition (Re=2300). This maximum increases with decreasing pipes diameter. A local minimum of entropy generation is also observed in transitional regime for Reynolds numbers around 6000. This local minimum is reached when the decrease of the entropy generation caused by thermal transfer tends to be countered by the increase of the entropy generation due to viscous dissipation. For lower heat exchanger area (large Reynolds number), the entropy generation due to the viscous dissipation exceeds that of heat transfer, and consequently the total entropy generation increases sharply.

As the optimal design for low Reynolds number can not be considered as realistic because of its high footprint, it seems to be interesting to propose a heat exchanger design with Reynolds number around 6000, corresponding to the local minimum of the entropy generation observed for transitional regime.

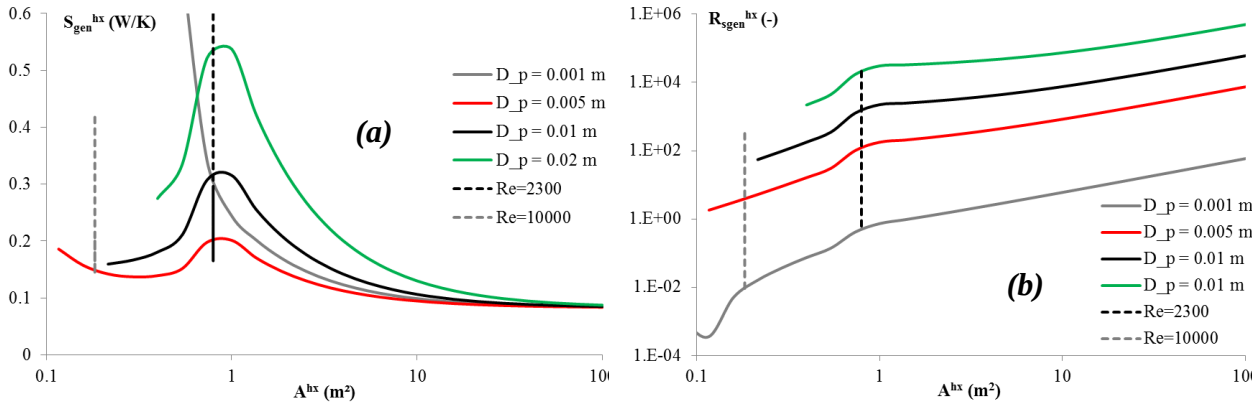

Fig. 2. Heat exchanger analysis. (a) Entropy generation rate in the heat exchanger vs the heat exchanger footprint, for different pipe diameter, (b) Entropy generation ratio in the heat exchanger vs the heat exchanger footprint, for different pipe diameter.

3.3. Thermoelectric module analysis

In this part, the optimization problem could be reduced to design a thermoelectric module coupled to its heat sources by a given thermal resistance R_{th} (heat exchanger design not considered here). The thermoelectric module design analysis is performed to reach the maximum COP for a given hot useful thermal power Q_h^*. As the thermal power demand Q_h^* and the source temperatures are assumed to be known, set a thermal resistance gives the thermoelectric junction temperatures T_h^{TE} and T_c^{TE} (derived from eq. 4 for maximum COP).

The simulations of the thermoelectric module have been done considering a hot thermal power $\left(Q_h^*\right)$ equal to 3000 W and temperature for the hot and the cold sources equal respectively to 303.15 K and 278.15 K.The design variables considered in this part are restricted to the thermoelectric module (the legs number N_L, their length L_L and section A_L and the electric current I). The optimization problem can be partly solved thanks to the following analytical considerations. The optimal intensity that gives the maximum COP is derived analytically with $\partial COP / \partial I = 0$:

$$I^* = \frac{K \cdot \Delta T}{\alpha_m \cdot T_m}\left(1+M\right) \tag{16}$$

With $M = \sqrt{1+Z \cdot T_m}$ and $Z = \frac{\alpha_m{}^2}{\rho \cdot \lambda}$, thermoelectric material constants.

Obviously, the maximum COP is reached when the entropy generation is minimum, according to (6): $\mathrm{Max}(COP) = \mathrm{Min}(S_{gen}^{TE})$. Consequently, the optimal electric current I^* leads to maximize the system performance and also to minimize the dissipation phenomena.

As the operating temperatures and the material properties are supposed to be known, this equation links the optimal electric current I^* to the optimal leg's length $L_L{}^*$ and optimal section $A_L{}^*$ via the constant ratio R_1^{TE}:

$$R_1^{TE} = \frac{I^* \cdot L_L^*}{A_L^*} = \frac{\lambda \cdot \Delta T}{\alpha_m \cdot T_m}\left(1+M\right) \tag{17}$$

In this condition, the maximum COP is given by:

$$COP^* = \frac{T_m}{\Delta T}\left(\frac{M-1}{M+1}\right)+\frac{1}{2} \tag{18}$$

Note that this value only depends on the thermoelectric material properties and the operating junction temperatures. That is to say, the maximum *COP* can be reached for any useful thermal power $\left(Q_h^*\right)$. Consequently, the minimum entropy generation reachable is also independent of the thermoelectric design. Figure 3(a) plots the evolution of the maximum *COP* and the minimum entropy generation vs the thermal resistance of the heat exchangers, for different leg length. The results confirm that the maximum *COP* and the minimum S_{gen} are not a function of the leg length (and the corresponding optimal design), but depend only on the thermoelectric properties and the thermal resistances that set the junction temperatures for given source temperatures and a given thermal demand. Obviously, the entropy generation increases as the thermal resistances of the heat exchangers increase. Indeed, as the source temperatures are given, an increase of the thermal resistance results in an increase of the junction temperature difference that decreases the system performances.

For further analysis on the dissipative phenomena, both dissipative contributions in the thermoelectric module (conduction and Joule effect) are plotted in figure 3(b). As expected, the entropy generation associated to conduction in the module increases with the increase of the junction temperature difference (for increasing thermal resistance). To reach useful thermal power $\left(Q_h^*\right)$. , the optimal conditions need a higher electric current for higher thermal resistance, resulting in higher dissipation by Joule effect in the module. In these operating conditions, the Joule dissipation exceeds the conduction dissipation, as shown by the plotted ratio $S_{gen}^{Joule}/S_{gen}^{Cond}$ in figure 3(b). However, this ratio tends to decrease for high thermal resistance, because conduction dissipation increases more strongly than Joule effect dissipation.

Furthermore, the thermoelectric design has to cover the optimal heating power given by:

$$Q_h^* = \frac{N_L \cdot K \cdot \Delta T}{T_m}\left[T_h\left(M+1\right)+\frac{\Delta T}{2}\frac{\left(M+1\right)}{\left(M-1\right)}-T_m\right] \tag{19}$$

It follows that the optimal electric current I^* and the optimal legs number $N_L{}^*$ are linked by the following constant ratios R_2^{TE} and R_3^{TE} :

$$R_2^{TE} = I^* \cdot N_L^* = \frac{Q_h^* \cdot \left(M+1\right)}{\alpha_m \cdot \left[T_h\left(M+1\right)+\frac{\Delta T}{2}\frac{\left(M+1\right)}{\left(M-1\right)}-T_m\right]} \tag{20}$$

$$R_3^{TE} = \frac{L_L^*}{A_L^* \cdot N_L^*} = \frac{\lambda \cdot \Delta T}{Q_h^* \cdot T_m}\left[T_h\left(M+1\right)+\frac{\Delta T}{2}\frac{\left(M+1\right)}{\left(M-1\right)}-T_m\right] \tag{21}$$

Any thermoelectric module design that respects the previous ratios R_1^{TE}, R_2^{TE} and R_3^{TE} will meet the useful thermal power $\left(Q_h^*\right)$. with maximum COP [18]. Similar expressions including Thomson effect are given in [19]. The evolution of these three ratios are plotted vs the thermal resistance in figure 3(c), as the thermal resistance modifies the junction temperatures for given sources temperature. These ratios remain almost constant while the thermal resistance is below 1.10^{-3} K/W, for the operating conditions considered.

Since the cost of THPs is strongly related to the thermoelectric material, we suggest seeking the thermoelectric system requiring the minimum volume V of thermoelectric material. V is defined by $V = N_L \cdot L_L \cdot A_L$. Combining with (21) gives:

$$V = \frac{Q_h^* \cdot T_m}{\lambda \cdot \Delta T \cdot \left[T_h (M+1) + \frac{\Delta T}{2} \frac{(M+1)}{(M-1)} - T_m \right]} \cdot L_L^{*2} \qquad (22)$$

In conclusion, minimizing the leg length minimizes the thermoelectric material volume (and thus its cost) for optimal operating conditions. Consequently, the authors propose to set the leg length to a minimum value based on technology feasibility. Considering manufacturing limitations, the minimum leg length L_L has been set to 1 mm. To confirm this analysis, the total thermoelectric area ($A_{TE} = N_L A_L$) is plotted for different leg length in figure 3(d). The results show that the total thermoelectric area decreases linearly with decreasing leg length. Consequently, the thermoelectric material volume decreases proportionally to the square of the leg length, as given by (22).

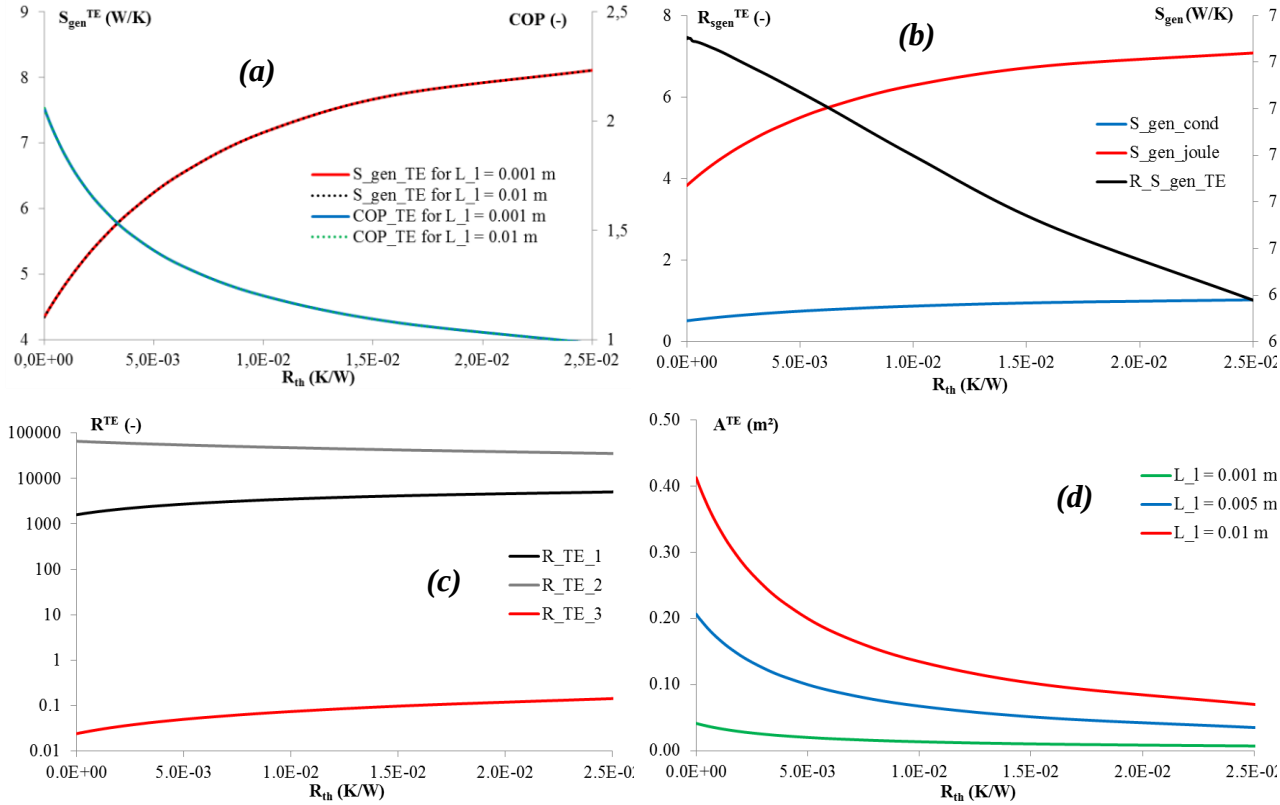

Fig. 3. Thermoelectric module analysis. (a) Entropy generation rate and COP of the thermoelectric module vs the thermal resistance for different leg length, (b) Entropy generation by conduction and Joule effect and their ratio vs the thermal resistance, (c) Optimal design ratios vs the thermal resistance, (d) thermoelectric module area vs the thermal resistance for different leg length.

3.4. Whole system analysis

Based on sensibility and optimization analysis performed on the heat exchangers and on the thermoelectric module, an optimization of the whole system design has been carried out. For this analysis, the design of the heat exchanger has been set with the nominal value used for the parametric study on that component and for the thermoelectric module the length of the legs has been set to 1 mm. The operating conditions considered for this analysis are those introduced in the table 2. The optimization procedure has been performed with the section of the thermoelectric legs as optimization variable and minimized the total entropy generation as objective function.

The figure 4(a) shows the total entropy generated in the whole system in function of the heat exchanger area. Once again, the minimum total entropy generation is reached for the higher heat exchanger area. The two local maximum of entropy generation correspond to laminar/transitional regime transition in the two heat exchangers (fig. 4(a)). The figure also highlights the presence of a local minimum of the entropy generation for transitional regime in the heat exchangers. The figure 4(b) points out that the major part of the entropy generation takes place in the thermoelectric module. In that component the most dissipating phenomenon is still the joule effect. The hot heat exchanger generates more entropy than the cold one because of the higher thermal power exchanged with the thermoelectric module (fig 4(b)). As already discussed, the entropy generation due to the viscous dissipation is low compared to that generated by the heat transfer, except for the small heat exchanger surfaces.

Although the entropy generation in the heat exchangers is low compared to that in the thermoelectric module, the global system performance is widely dependent of the junction temperatures, and thus of the thermal resistances of the heat exchangers. This coupling is discussed in the thermoelectric module analysis and is highlighted by the entropy generation variation in the whole system corresponding to the laminar-transitional regime transition in the heat exchanger pipes.

The figure 4(a) also shows the area ratio $\left(R_A = A_{hx} / A_{TE} \right)$ which increases with the rise of the heat exchanger area. Although the lower entropy generation of the whole system is reached at the maximum heat exchanger area that design can not be considered as a realistic design of a thermoelectric heat pump because of its high footprint. Additional thermal constriction resistances have to be taken into account to transfer heat flux from the thermoelectric surface area to the heat exchangers basis area. Considering the footprint of the system it seems to be interesting to propose a design with an area ratio around 4, corresponding to the local minimum of the entropy production for transitional regime in the heat exchangers.

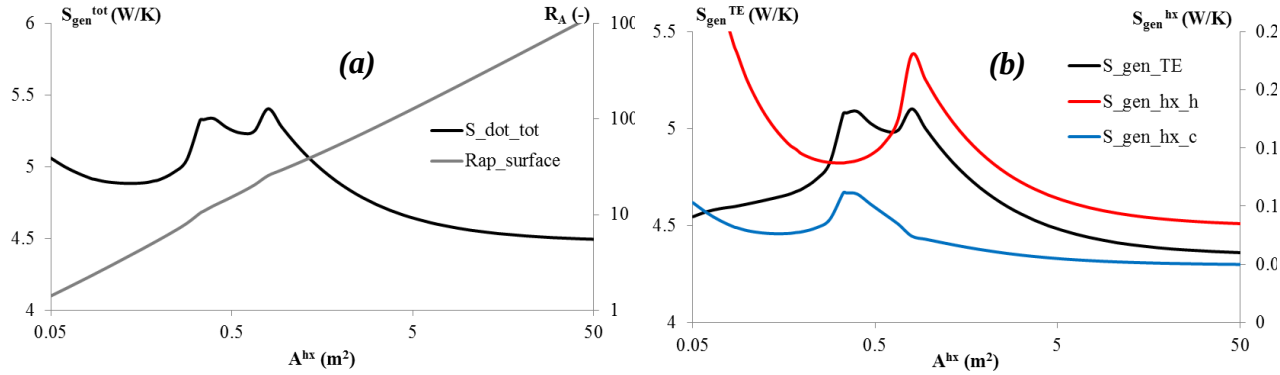

Figure 4. Whole system analysis. (a) Entropy generation rate and area ratio vs the heat exchanger footprint, (b) Entropy generation rates in each component of the system vs the heat exchanger footprint.

The entropy flows inside the system and with its sources for that specific design are plotted in figure 5. As already discussed that diagram highlights that the higher dissipative phenomenon is the joule effect in the thermoelectric legs.

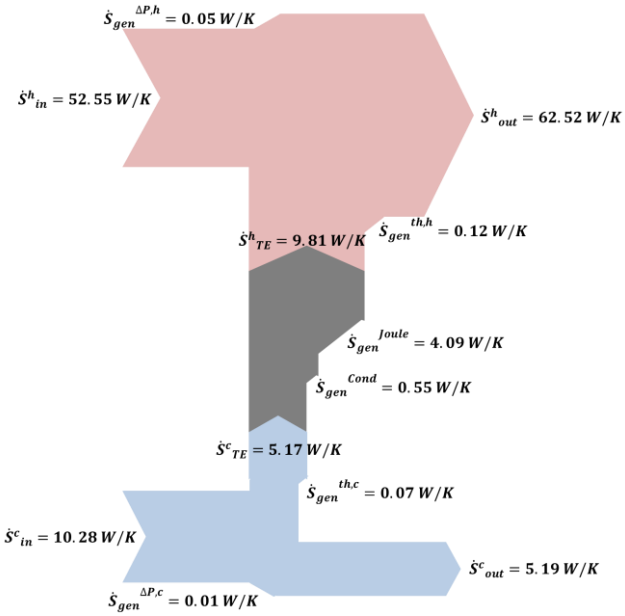

Fig. 5. Entropy flow through the system for optimal design.

4. Conclusion

This papers aims to propose a design strategy for water/water thermoelectric heat pump with high performance based on thermodynamic analysis. The system studied is composed of a thermoelectric module sandwiched between the hot and cold heat exchangers to transfer heat from the thermoelectric junctions to the sources. This study assumes that the thermoelectric material and fluid properties are known. The operating conditions, such as the inlet/outlet temperatures in both heat exchangers and the thermal demand, have to be defined. The design variables considered in this study are the number of thermoelectric legs N_L, their length L_L, and section A_L for the thermoelectric module, and the number of channel $N_{h/c}$, their diameter $D_{h/c}$ and their length L for both heat exchangers.

A second law analysis allows distinguishing and quantifying each dissipative phenomenon occurring in the system: Joule effect and thermal conduction in the thermoelectric module, and viscous friction and thermal transfer in both heat exchangers. Three optimal design ratios for the thermoelectric module are highlighted thanks to analytical considerations. As the total thermoelectric material volume is linked to the leg length (in optimal conditions), the authors propose to reduce as possible its value, with respect to the manufacturing process. The heat exchangers analysis confirms that the optimal design is reached for low Reynolds number (laminar flow), meaning a high footprint. A local minimum of the entropy generation rate is also observed for transitional regime ($Re \sim 6000$), that helps to reduce the heat exchangers footprint. When considering the whole system, entropy generation rate in the thermoelectric module highly dominates those in the heat exchangers, mainly because of Joule effect. However, the heat exchangers design highly impacts the global THP performances, as the thermoelectric junction temperatures depends on the heat exchanger design. Realistic optimal design can be reached when the heat exchanger footprint is around 4 times higher than the total thermoelectric module area, for the operating conditions considered. This realistic optimal design corresponds to the local minimum of the entropy generation rate for transitional regime in the heat exchangers.

Nomenclature

A	area, m²	D	channel diameter, m
Cp	specific heat, J/(kg K)	f	friction factor, -
COP	coefficient of performance, -	h	heat transfer coefficient, W/(m² K)

I	electric current, A	R	electric resistance, Ω
K	thermal conductance, W/K	R_{th}	thermal resistance, W/K
L	length, m	Re	Reynolds number, -
$\dot{m}$	mass flow rate, kg/s	S	entropy flow, W/K
N	Number of channels/legs, -	S_{gen}	entropy generation rate, W/K
Nu	Nusselt number, -	T	temperature, K
P	pressure, Pa	v	velocity, m/s
Pr	Prandtl number, -	Z	figure of merit, 1/K
Q	thermal power, W		

Greek symbols

α	Seebeck coefficient, V/K	ρ	electric resistivity, Ω.m
λ	thermal conductivity, W/(m K)	μ	viscosity, Pa.s

Subscripts and superscripts

in	inlet	hx	heat exchanger
out	outlet	Cond	conduction
c	cold	Joule	Joule effect
h	hot	th	thermal transfer
TE	thermoelectric module	ΔP	viscous dissipation

References

~~[1] Chang Y. W., Chang C. C., Ke M. T., and Chen S. L., Thermoelectric air-cooling module for electronic devices. Applied Thermal Engineering, 2009. 29(13): p. 2731-2737.~~

~~[2] Chatterjee S., Purkait P.K., and Garg D., Athermalization of infra-red camera of projectile weapons. Applied Thermal Engineering, 2009. 29(10): p. 2106-2112.~~

[3] ~~Rowe D.M., Applications of nuclear-powered thermoelectric generators in space. Applied Energy, 1991. 40(4): p. 241-271.~~

[4] Riffat S.B. and Ma X., Thermoelectrics: a review of present and potential applications. Applied Thermal Engineering, 2003. 23(8): p. 913-935.

[5] Rowe D. M., CRC Handbook of Thermoelectrics, 3rd ed., CRC Press, Boca Raton, USA, 1995.

[6] Kim Y.W., Ramousse J., Fraisse G., Dalicieux P., and Baranek P., Optimal sizing of a thermoelectric heat pump (THP) for heating energy-efficient buildings. Energy and Buildings, 2014. 70: p. 106-116.

[7] David B., Ramousse J., and Luo L., Optimization of thermoelectric heat pumps by operating condition management and heat exchanger design. Energy Conversion and Management, 2012. 60: p. 125-133.

[8] Le Pierrès N., Cosnier M., Luo L., and Fraisse G., Coupling of thermoelectric modules with a photovoltaic panel for air pre-heating and pre-cooling application ; an annual simulation. International Journal of energy research, 2008. 32: p.1316-1328.

[9] Cosnier M., Fraisse G., and Luo L., An experimental and numerical study of a thermoelectric air-cooling and air-heating system. Int. Journal of refrigeration, 2008. 31: p. 1051-1062.

[10] Goupil C., Seifert W., Zabrocki K., Muller E., and Snyder G. J., Thermodynamics of Thermoelectric Phenomena and Applications. Entropy, 2011. 13: p. 1481-1517.

[11] Pan Y., Lin B., and Chen J., Performance analysis and parametric optimal design of an irreversible multi-couple thermoelectric refrigerator under various operating conditions. Applied Energy, 2007. 84: p. 882-892.

[12] Lee K.H., and Kim O.J., Analysis on the cooling performance of the thermoelectric micro-cooler. International Journal of Heat and Mass Transfer, 2007. 50: p. 1982-1992.

[13] Feidt M., Thermodynamique optimale en dimensions physiques finies. Hermes Science Publications; 2013. ISBN: 9782746245426.

[14] Ioffe A.F., Semiconductor thermoelements and thermoelectric cooling. London, UK: Infosearch ltd.; 1957.

[15] Yamashita O., Effect of the temperature dependence of electrical resistivity on the cooling performance of a single thermoelectric element. Appl. Energy, 2008. 85: p. 1002-1014.

[16] Riffat S.B., Ma X., and Wilson R., Performance simulation and experimental testing of a novel thermoelectric heat pump system. Applied Thermal Engineering, 2006. 26: p. 494-501.

[17] F.P. Incropera, D.P. DeWitt, Fundamentals of heat and mass transfer, 5th ed. New York: J. Wiley; 2002.

[18] Ramousse J., Sgorlon D., Fraisse G., Perier-Muzet M., Analytical optimal design of thermoelectric heat pumps. Applied Thermal Engineering, 2015. 82: p.48–56

[19] Sgorlon D., Fraisse G., and Ramousse J., Theoretical optimal operating conditions for thermoelectric cooler, including Thomson effect. Proceedings in Congrès Français de Thermique 2011, Energie Solaire et Thermique, 24-27 Mai 2011, Perpignan, France, p.807-812.

[20] A. Rezaniaa, K. Yazawab, L.A. Rosendahla, A. Shakourib, Co-optimized design of microchannel heat exchangers and thermoelectric generators. International Journal of Thermal Sciences, 2013. 72 : p. 73–81